Magnetism induced by single carbon vacancies in a three-dimensional graphitic network

R. Faccio,[1] H. Pardo,[1] P. A. Denis,[1] R. Yoshikawa Oeiras,[2] F. M. Araújo-Moreira,[2] M. Veríssimo-Alves,[3] and A. W. Mombrú[1]
[1]*Crystallography, Solid State and Materials Laboratory (Cryssmat-Lab), DETEMA, Facultad de Química, Universidad de la República, P.O. Box 1157, Montevideo 11800, Uruguay*
[2]*Departamento de Física, Universidade Federal de São Carlos, Caixa Postale 676, São Carlos, São Paulo CEP 13565-905, Brazil*
[3]*The Abdus Salam International Centre for Theoretical Physics, Strada Costiera 11, Main Building, Trieste I-34014, Italy*
(Received 18 December 2006; revised manuscript received 12 September 2007; published 15 January 2008)

We present an *ab initio* density functional theory study of the magnetic moments that arise in graphite by creating single carbon vacancies in a three-dimensional (3D) graphite network using full potential, all electron, spin polarized electronic structure calculations. In previous reports, the appearance of magnetic moments was explained in a two-dimensional graphene sheet just through the existence of the vacancies itself [*Carbon-Based Magnetism*, edited by F. Palacio and T. Makarova (Elsevier, Amsterdam, 2005); D. C. Mattis, Phys. Rev. B **71**, 144424 (2005); Y. Kobayashi *et al.*, *ibid.* **73**, 125415 (2006); R. Yoshikawa Oeiras *et al.*, *ibid.* (to be published); P. O. Lehtinen *et al.*, Phys. Rev. Lett. **93**, 187202 (2004)]. The dependence of the arising magnetic moment on the nature and geometry of the vacancies for different supercells is reported. We found that the highest value of magnetic moment is obtained for a $3\times3\times1$ supercell and that the highly diluted $5\times5\times1$ supercell shows no magnetic ordering. The results obtained in this paper are indicative of the importance of interlayer interactions present in a 3D stacking. We conclude that this should not be underestimated when vacancy-based studies on magnetism in graphitic systems are carried out.

DOI: 10.1103/PhysRevB.77.035416 PACS number(s): 81.05.Uw, 71.15.Ap, 71.15.Mb, 75.50.Dd

I. INTRODUCTION

Carbon-based materials have attracted the attention of the scientific community due to their many potential technological applications. For this reason, novel properties induced on graphite by chemical or physical modifications have become a subject of great interest.[1–5] Many theoretical articles focus not only on the defects of nanostructured materials but also in the contour edges or in the presence of other atoms.[2–5] In most of them, the system was modeled as an interaction among atoms within a graphene (single graphite layer). In this paper, we are studying the effect of the presence of single atom vacancies in a three-dimensional graphitic network, bulk graphite, with different supercells, with emphasis on the metallic nature and the magnetic response of this modified material.

II. METHODOLOGY

The *ab initio* calculations were performed within the density functional theory (DFT) framework using full potential, all electron, spin polarized electronic structure calculations utilizing the augmented plane wave (APW)+local orbital (lo) method within the WIEN2K code.[6] For the exchange-correlation potential, we used generalized-gradient approximation (GGA) in the Perdew-Burke-Ernzerhoff (PBE) scheme.[7] Scalar relativistic effects were included, but spin-orbit coupling was neglected.

The convergence of the basis set is controlled by a cutoff parameter expressed as the product between the smallest muffin-tin radius in the unit cell (R_{MT}) and the magnitude of the maximum reciprocal lattice vector (K_{max}). The muffin-tin radii for carbon atoms were selected as $R_{MT}=1.25$ a.u., achieving convergence for a cutoff value of $R_{MT}K_{max}=5.5$. The $1s$ state was selected as a core state, while the $2s$ and $2p$ states were treated as valence states. In all the cases, the valence charge densities were expanded up to a G_{max} value of 20.0 a.u.$^{-1}$, equivalent to kinetic energy $E_{cut}=400$ Ry, in order to increase the accuracy in the determination of the topology of the electronic density. Finally, the k-point sampling in the first Brillouin zone was determine specifically for each supercell (Table I), studying convergence for different numbers of density points. In the case of pristine graphite, we obtain a convergence in total energy with 16 000 points in the entire first Brillouin zone.

Layered materials present strong corrugation of the crystal potential in the direction perpendicular to the layers. Since this is the case of bulk graphite, the local-density-approximation (LDA) exchange-correlation potential does not accurately reproduce the crystal potential of this system. For example, it is known that LDA tends to overestimate interlayer interactions in graphite, leading to slightly short distances along its c direction or, in some cases, leading by chance close to the experimental one. For this reason, some reports support that the GGA exchange-correlation (xc) potential is more adequate in systems with important inhomogeneities on their charge densities along the direction perpendicular to the c axis[8–10] and for the reconstruction in the a-b plane. They postulate the use of this potential instead of a LDA approach, since they find it more appropriate for carbon structures. Although the van der Waals forces are totally neglected[11] for both xc potentials, GGA leads to an increase of the interlayer distances, which causes that some authors prefers to use the LDA potential.[5–10,12] We present here the results of the supercell series using the GGA potential and compare the results extracted from calculations using LDA and GGA for the $3\times3\times1$ supercell, in order to support the reliability of the conclusions presented in this paper.

Graphite is a nonmagnetic semimetal that displays a very weak dispersion along the c axis. We started from the hexagonal graphite cell in the $P6_3/mmc$ space group, A-B stack-

TABLE I. Total magnetic moments for the different supercells, relaxed (RC) and nonrelaxed (NRC), indicating in each case the number of k points in the entire first Brillouin zone (N-kpts).

Supercell SC	No. of atoms	Relaxed c (a.u.)	N-kpts for NRC	MM for NRC (μ_B)	MM for RC (μ_B)	N-kpts for NRC
$1\times1\times1$	4	15.50	16 000	0.00	0.00	16 000
$2\times2\times1$	14	16.00	16 000	0.63	2.01	16 000
$3\times3\times1$	34	14.90	3200	1.76	2.06	3200
$3\times3\times1$[a]	34	12.50	···	···	1.40	3200
$3\times3\times1$[b]	34	14.65	···	···	2.21	3200
$4\times4\times1$	62	15.11	1600	1.41	1.21	800
$5\times5\times1$	98	15.68	400	0.00	0.00	400

[a]APW+lo results for the $3\times3\times1$ supercell using LDA as a xc-potential.
[b]LCNAO (SIESTA code) results for the case of $3\times3\times1$ supercell.

ing, $a_0=b_0=4.656$ a.u. and $c_0=12.682$ a.u., and constructed a series of supercells. Then, we removed single atoms on each graphene layer, in order to obtain vacancies aligned along the c axis, the $(0,0,\frac{1}{4})$ and $(0,0,\frac{3}{4})$, in different concentrations by means of different volumes of the supercells (Fig. 1).[13] After this, we performed a spin polarized calculation with geometrical relaxation of the atomic positions. This last step was carried out minimizing the forces in the atoms and the total energy of the system. In all the cases, the force tolerance was selected as 1.0 mRy/a.u. This process was repeated for different c values until the one that minimizes the total energy is found; this is called the equilibrium result c_{eq}. In order to check that the ground state of the systems is magnetic, we forced the system to converge to a nonmagnetic solution, as in pristine graphite, and we found in all the cases a solution with higher energy than in the magnetic one (except for the $5\times5\times1$ supercell, as will be shown below).

The localized states along the c axis (see Figs. 2 and 3), could be related to the possible spontaneous magnetism of the material in agreement with previous reports.[4,5] The relaxation of the atoms within each supercell is an important effect that was taken into account in this study. Table I shows the final total magnetic moment for the different supercells.

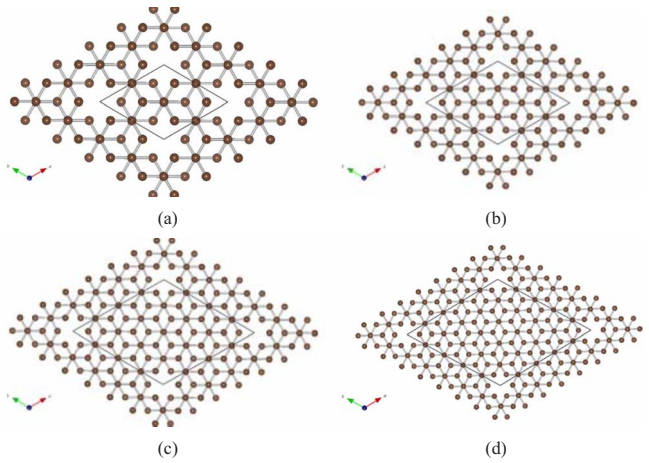

FIG. 1. (Color online) Sketch for the (a) $2\times2\times1$, (b) $3\times3\times1$, (c) $4\times4\times1$, and (d) $5\times5\times1$ supercells showing the A-B stacking of layers.

III. RESULTS AND DISCUSSION

A. 2×2×1 supercell

The $2\times2\times1$ supercell corresponds to the more defective material. It exhibits metallic behavior with two bands, for each polarized case, being crossed at the Fermi level. The magnetic moment arrangement is ferrimagnetic; the spin density map of Figs. 2(a) and 2(b) shows the major p_z character of the charge ordering. In particular, the spin density is higher for atoms near the vacancy and it decays when moving away from it. Thus, the spin configuration of the system is ferrimagnetic, with higher spin-up charge in comparison to the spin-down one. As it would be expected, the c_{eq} relaxed axis is longer than the experimental c_0 value in graphite, and it is slightly larger than the predicted one, by DFT-GGA, in pure graphite where the c axis was optimized obtaining a final value of $c=15.50$ a.u. The total magnetic moments were $0.63\mu_B$ for the nonrelaxed cell and $2.01\mu_B$ for the relaxed case.

B. 3×3×1 supercell

The $3\times3\times1$ supercell presents a metallic behavior and shows magnetic response too. The energy band structure shows six up-electron energy bands and four down-electron energy bands that cross the Fermi level. The magnetic response could be due to these localized states, which can be confirmed too by inspection of its density of states [Fig. 3(a)]. The $c_{eq}=14.90$ a.u. relaxed axis is longer than the experimental c_0 value in graphite, but it is slightly shorter than the predicted one by DFT-GGA in pure graphite where the c axis was optimized obtaining a final value of $c=15.50$ a.u. This trend could be in relation with some experimental findings where x-ray diffraction experiments showed that modified magnetic graphite tends to decrease the $(00l)$ interlayer spacing.[14,15] Another point related with the electronic structure is the dispersion of the bands, in particular, in the Γ-A direction (Fig. 4), which is appreciable even in the case of overestimation of the c-axis length ($c_{eq}=14.90$ a.u.). This

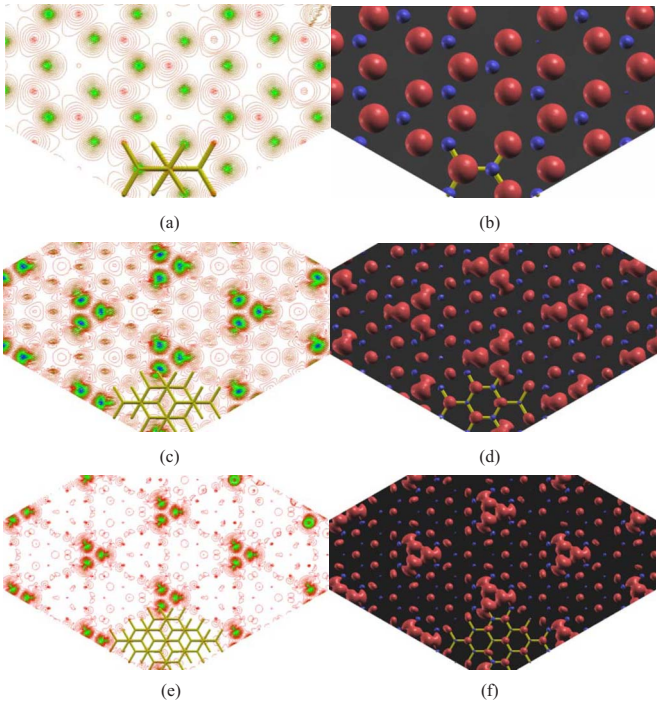

FIG. 2. (Color online) (a) Spin density map for the $2\times2\times1$ supercell in the range $\delta\rho_\sigma=0.070\sigma/\text{a.u.}^3$ and $-0.012\sigma/\text{a.u.}^3$, (b) respective isosurface evaluated at $\delta\rho_\sigma=\pm5.0\times10^{-3}\sigma/\text{a.u.}^3$, (c) spin density for $3\times3\times1$ supercell in the range $\delta\rho_\sigma=0.052\sigma/\text{a.u.}^3$ and $-0.005\sigma/\text{a.u.}^3$, (d) isosurface for $3\times3\times1$ supercell for $\delta\rho_\sigma=\pm2.5\times10^{-3}\sigma/\text{a.u.}^3$, (e) spin density for $4\times4\times1$ supercell in the range $\delta\rho_\sigma=0.069\sigma/\text{a.u.}^3$ and $-0.002\sigma/\text{a.u.}^3$, and (f) Isosurface for $4\times4\times1$ supercell for $\delta\rho_\sigma=\pm8.0\times10^{-4}\sigma/\text{a.u.}^3$. The spin density is expressed as $\delta\rho_\sigma(\vec{r})=\rho_\uparrow(\vec{r})-\rho_\downarrow(\vec{r})$. The most positive values are represented in blue, while the most negative are in red according to each range.

band is almost filled for the spin-down electrons, showing a positive slope along Γ-*A*, which could be related with the tendency of contraction of the *c* axis. This characteristic reinforces the importance of regarding this material as a real three-dimensional (3D) crystal. The total magnetic moment for this supercell increases from $1.76\mu_B$ to $2.06\mu_B$ when the *c* axis is optimized. The spin arrangement is again ferrimagnetic, with a spin density which is mainly due to p_z orbitals for atoms far from the vacancy [Figs. 2(c) and 2(d)]. An important difference with the $2\times2\times1$ supercell case is that a strong component of sp^2 hybridization in the region near the vacancy is observed. These three lobules are connected symmetrically between them, with some degree of saturation. This can be deduced for the magnetic moment per vacancy which is $1.06\mu_B$ in the case of the c_{eq}, in close agreement with earlier reports.[4]

C. 4×4×1 supercell

The $4\times4\times1$ supercell yields again a metallic and magnetic material. Here, the system shows metallic behavior with one and two bands being crossed by the Fermi level in the case of spin-up and -down electrons, respectively. A difference to the previous case is that although showing some

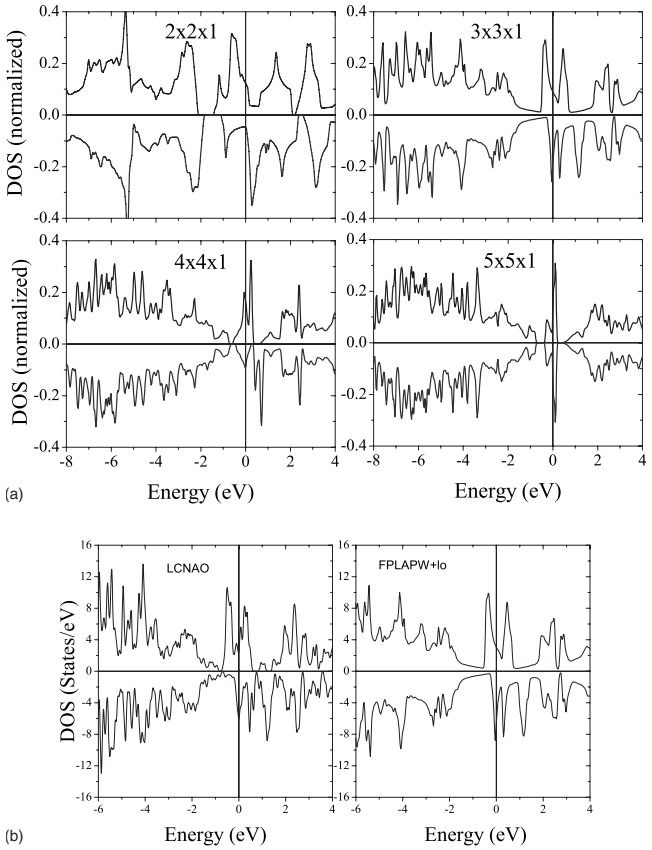

FIG. 3. (a) Density of states for the $2\times2\times1$, $3\times3\times1$, $4\times4\times1$, and $5\times5\times1$ relaxed supercell. Density of states is expressed as states and/or eV and/or number of atoms in supercell. (b) Comparison between LCNAO (SIESTA code) and APW+lo (WIEN2K code) results for the $3\times3\times1$ supercell.

dispersion, no bands cross the Fermi level along the Γ-*A* path. The spin density shows similarities with the $3\times3\times1$ case, where the ferrimagnetic order is mainly based on the p_z spin density far from the point defect, and a strong localization of charge associated with sp^2 orbitals in vicinity of the vacancy. For this case, the total magnetic moment decreases when the *c* axis is optimized. These moments are $1.41\mu_B$ and $1.21\mu_B$ for c_0 and c_{eq} (15.11 a.u.), respectively. This fact could be explained in terms of the stability reached in the presence of local magnetic field. In this case, there are no bands crossing the Fermi level along the Γ-*A* path, so the stabilization energy addressed for the *c*-axis contraction (more dispersion) is not as remarkable as it was in the case of the $3\times3\times1$ supercell. For this reason, the c_{eq} is higher than in the $3\times3\times1$ case.

D. 5×5×1 supercell

The $5\times5\times1$ supercell is different from the other ones since it is a semimetal, with a negligible amount of states per energy at the Fermi level. Since the system exhibits nonmagnetic response, the c_{eq} is close to that of the pristine graphite, 15.67 and 15.50 a.u., respectively. This is another point that reinforces the structural and electronic correlations in this magnetic system.

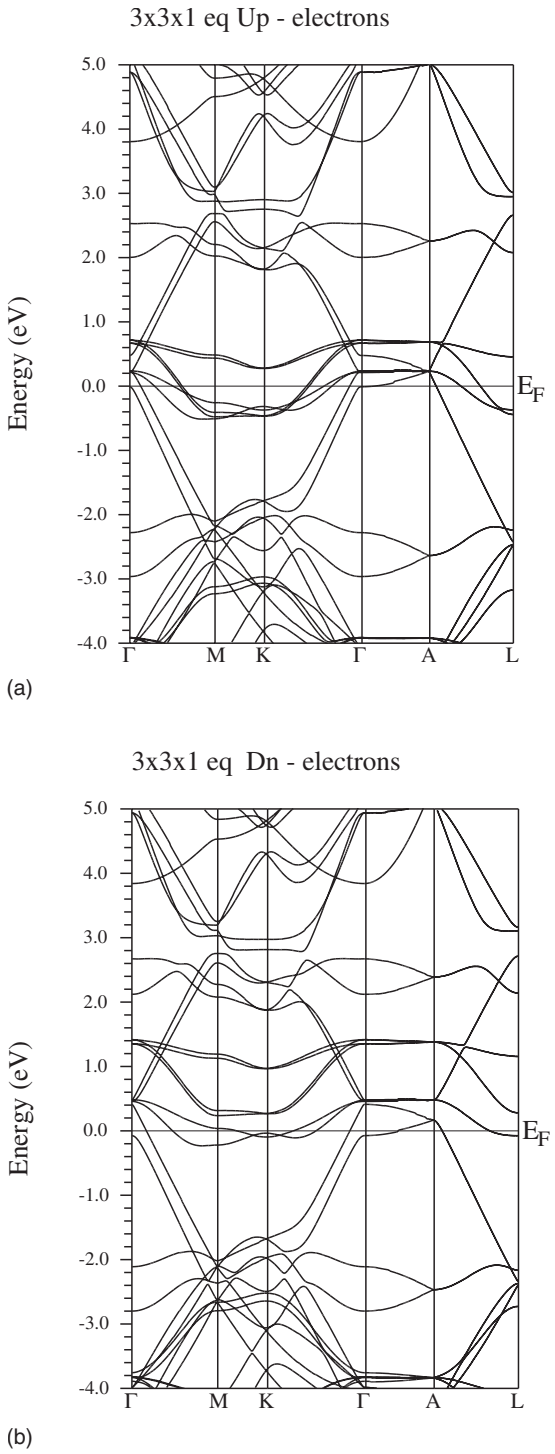

FIG. 4. (a) Spin-up and (b) -down electrons energy band structures for the $3\times3\times1$ supercell.

E. Local-density-approximation exchange-correlation potential for the 3×3×1 supercell

The calculations performed using LDA potential for the $3\times3\times1$ supercell yielded a magnetic moment of $1.40\mu_B$ for a graphitic structure with $c_{eq}=12.50$ a.u. This distance is in good agreement with the one obtained for pristine graphite using the LDA xc potential $c_{eq}=12.55$ a.u. Even when shifting away from the equilibrium value from the c axis, the magnetic behavior was still present for this supercell. The magnetic moment ranges from $1.39\mu_B$ to $1.42\mu_B$ for c-axis values between 12.30 and 12.70 a.u., with a positive slope. Although a cell contraction is verified in comparison with the results obtained using GGA, as expected, this fact does not imply a significant variation in the magnetic behavior of the system, which is the main focus of this paper.

F. Linear combination of numerical atomic orbitals (LCNAO) for the 3×3×1 supercell and single graphene sheet

In order to check our APW+lo results, we performed for the $3\times3\times1$ supercell another *ab initio* approach using the SIESTA code,[16–18] which adopts a linear combination of numerical localized atomic-orbital basis sets for the description of valence electrons and norm-conserving nonlocal pseudopotentials for the atomic core. The pseudopotentials were constructed using the Troullier-Martins scheme[19] which describes the interaction between the valence electrons and atomic core. The total energy was calculated within the PBE form of GGA.[7] The real-space grid used to represent the charge density and wave functions was the equivalent of that obtained from plane-wave cutoff of 300 Ry, the atomic positions were fully relaxed using a conjugate-gradient algorithm[20] until a force of 1.6×10^{-3} Ry/a.u., and a maximum stress component of 0.05 GPa was reached. A Monkhorst-Pack grid[21] with a $20\times20\times19$ supercell, defined in terms of the actual supercell, was selected to obtain a mesh of 3200 k points in the full Brillouin zone. This process was repeated for different c-axis values without applying basis set superposition error correction to find the equilibrium result at $c_{eq}=14.65$ a.u. with a total magnetic moment in cell of $2.21\mu_B$, which are in close agreement with the results obtained by the APW+lo method, with $c_{eq}=14.90$ a.u. and a magnetic moment of $2.06\mu_B$. The density of the occupied states obtained by both codes [Fig. 3(b)] shows similarities in the electronic structure, in particular, for those states near the Fermi level. The final atomic positions are in close agreement, and no distortion for the flat sheet geometry is observed.

In order to check the reliability of this result, we performed further calculations using the SIESTA code with a single graphene sheet for the 3×3, 4×4, and 5×5 supercell configurations. The distance between layers was selected as 15.00 a.u. in order to minimize the interactions among them. Identical conditions to the $3\times3\times1$ bulk supercell were applied for the initialization of the calculation. The only difference arises from the number of k points selected to sample the first Brillouin zone: 3200, 1600, and 800 for 3×3, 4×4, and 5×5, respectively. In all cases, these spin polarized calculations yielded flat sheets with a net magnetic moment, in agreement to what is here reported for the 3D stacking. These results are presented in Table II. However, differences in the symmetry of the environment surrounding the vacancies was not found for single graphene sheet but observed for the 3D stacking in the same supercell configurations. Experimental reports, using low temperature scanning tunneling microscopy, reveal the presence of a threefold organization

TABLE II. Total magnetic moments for the different supercells indicating the number of k points selected in the single graphene sheet calculations.

Supercell SC	No. of C atoms	N-kpts	MM (μ_B)
3×3	17	3200	2.00
4×4	31	1600	1.24
5×5	49	800	1.72

around point defects created on highly ordered pyrolytic graphite (HOPG).[22] We believe that this fact shows the key role of the interlayer interaction and the need to perform studies on the basis of a 3D graphitic network instead of single graphene sheets where the effect of the stacking is missed.

A deviation from the flatness was described in previous reports,[5,11] in disagreement with our results. In those articles, a pentagon that saturates two sp^2 orbitals was obtained when a single graphene sheet was optimized in its atomic positions, with different codes than the ones used in this paper. This pentagon let one of these sp^2 orbitals to contribute to the net magnetic moment. The structural distortion that the system undergoes sets this atom out of plane.

IV. CONCLUSIONS

We have investigated the magnetic order in a 3D graphitic system where single atom vacancies in different supercells were created. We found that the magnetism arising is accompanied by a metallic behavior and that the best configuration for such occurrence corresponds to the $3\times3\times1$ supercell, vanishing for the $5\times5\times1$ one.

The fact that the $5\times5\times1$ supercell does not show a net magnetic moment, while the 5×5 graphene supercell exhibits a magnetic moment of $1.72\mu_B$, reinforces the idea of the magnetism arising from a complex situation in which vacancies should interact with its images along the whole crystal. These results suggest that there is still work to do in experimental nanostructuration of graphite, trying to optimize the vacancy concentration and their geometrical configuration.

Additionally, to these electronic properties, there exist some structural correlations that were evidenced in early reports, in particular, the contraction of the c axis in the case of magnetic systems. The magnetic response found by creating single carbon vacancies in a 3D stacking using periodic supercells ranges between $0.02\mu_B$ and $0.14\mu_B$ per carbon atom, which is higher than the one found experimentally for defective bulk graphitic specimens, $(1.2\times10^{-3})\mu_B$ per carbon atom.[14,15] This fact would imply that by creating this supercell configuration, this theoretical study produces defects in a more densely way than what experiments can achieve. In order to go forward toward the theoretical simulation of what could happen when defective graphite is experimentally prepared,[14,15,23] further calculations using higher order vacancies have to be performed. In this work, which will be submitted soon, double or quadruple vacancies are created using different supercells. Although the calculations involved in this study are more expensive, they will provide more realistic results due to the incorporation of higher order vacancies.

Although beyond the scope of this research, a few words could be said about helium and hydrogen irradiation on HOPG samples.[23] The existence of intrinsic magnetism in a 3D graphitic network with regularly distributed vacancies could support the idea of the role of adsorption of hydrogen in the vacancies to enhance this magnetism, as previously discussed.[5] The adsorption of hydrogen, with eventual pinning in the defects, would have the effect of stabilizing the magnetic signal of the specimen by preventing the annihilation of the vacancies due to the recombination of Frenkel pairs, especially at room temperature. This would imply a remarkable advantage for hydrogen irradiation, in comparison to helium, which is supported by the experimental evidence, where hydrogen irradiated samples exhibit higher magnetic signal.[23] These ideas should be tested in a future work.

As a summary, an important result for the present paper was that flat graphene sheets, with a well defined symmetry for the atoms surrounding the vacancy, were obtained in all the 3D stacking cases, independently on the code or the potential used. All these properties, verified with two different *ab initio* codes, support the potential technological value of the nanostructured modified graphite in order to be considered in high-technology devices as a free metal material. We believe that the present paper contributes to rethink the role of the 3D stacking of graphene sheets in graphite and to stop disregarding this effect.

ACKNOWLEDGMENTS

We gratefully acknowledge PEDECIBA, CSIC, PDT (project 54/38), and DICYT—Fondo Clemente Estable (No. 10213) (Uruguayan organizations) for financial support. Ricardo Faccio would like to acknowledge PEDECIBA for a Ph.D. Grant.

[1] *Carbon-Based Magnetism*, edited by F. Palacio and T. Makarova (Elsevier, Amsterdam, 2005).
[2] D. C. Mattis, Phys. Rev. B **71**, 144424 (2005).
[3] Y. Kobayashi, K. I. Fukui, T. Enoki, and K. Kusakabe, Phys. Rev. B **73**, 125415 (2006).
[4] R. Yoshikawa Oeiras, F. M. Araujo-Moreira, M. Veríssimo-Alves, R. Faccio, H. Pardo, and A. W. Mombrú, Phys. Rev. B (to be published).
[5] P. O. Lehtinen, A. S. Foster, Yuchen Ma, A. V. Krasheninnikov, and R. M. Nieminen, Phys. Rev. Lett. **93**, 187202 (2004).
[6] P. Blaha, K. Schwarz, G. K. H. Madsen, D. Kvasnicka, and J. Luitz, WIEN2K, an augmented plane wave+local orbitals: Pro-

gram for Calculating Crystal Properties, Vienna University of Technology, 2001.
[7] J. P. Perdew, K. Burke, and M. Ernzerhof, Phys. Rev. Lett. **77**, 3865 (1996); **78**, 1396 (1997).
[8] V. N. Strocov, P. Blaha, H. I. Starnberg, M. Rohlfing, R. Claessen, J.-M. Debever, and J.-M. Themlin, Phys. Rev. B **61**, 4994 (2000).
[9] E. Konstantinova, S. O. Dantas, and P. M. V. B. Barone, Phys. Rev. B **74**, 035417 (2006).
[10] Y. Zhang, S. Talapatra, S. Kar, R. Vajtai, S. K. Nayak, and P. M. Ajayan, Phys. Rev. Lett. **99**, 107201 (2007).
[11] F. Tournus, J.-C. Charlier, and P. Mélinon, J. Chem. Phys. **122**, 094315 (2005).
[12] A. A. El-Barbary, R. H. Telling, C. P. Ewels, M. I. Heggie, and P. R. Briddon, Phys. Rev. B **68**, 144107 (2003).
[13] In all the cases of the supercells, the a and b parameters were generated as multiple of a_0 and b_0; the in-plane geometry of the cells was retained as a hexagonal. Only the atomic positions and c axis were optimized.
[14] H. Pardo, R. Faccio, F. M. Araújo-Moreira, O. F. de Lima, and A. W. Mombrú, Carbon **44**, 565 (2006).
[15] A. W. Mombrú, H. Pardo, R. Faccio, O. F. de Lima, E. R. Leite, G. Zanelatto, A. J. C. Lanfredi, C. A. Cardoso, and F. M. Araujo-Moreira, Phys. Rev. B **71**, 100404(R) (2005).
[16] P. Ordejón, E. Artacho, and J. M. Soler, Phys. Rev. B **53**, R10441 (1996).
[17] D. Sánchez-Portal, P. Ordejón, E. Artacho, and J. M. Soler, Int. J. Quantum Chem. **65**, 453 (1997).
[18] J. M. Soler, E. Artacho, J. D. Gale, A. García, J. Junquera, P. Ordejón, and D. Sánchez-Portal, J. Phys.: Condens. Matter **14**, 2745 (2002).
[19] N. Troullier and J. L. Martins, Phys. Rev. B **43**, 1993 (1991).
[20] W. H. Press, B. P. Flannery, S. A. Teukolsky, and W. T. Vetterling, *New Numerical Recipes* (Cambridge University Press, New York, 1986).
[21] H. J. Monkhorst and J. D. Pack, Phys. Rev. B **13**, 5188 (1976).
[22] J. G. Kushmerick, K. F. Kelly, H.-P. Rust, N. J. Halas, and P. S. Weiss, J. Phys. Chem. B **103**, 1619 (1999).
[23] P. Esquinazi, D. Spemann, R. Höhne, A. Setzer, K. H. Han, and T. Butz, Phys. Rev. Lett. **91**, 227201 (2003).